

A qualitative study of multiphase steel microstructure developed in four different steel alloys

W. Khraisat

The University of Jordan, Industrial Engineering Department, Amman, 11942, Jordan
w.khraisat@ju.edu.jo

(Received 19 February 2025; Accepted 04 July 2025)

Abstract

In this work, quench and partitioning (Q&P) heat treatment was performed on four different steel alloys in order to obtain multiphase steels having a microstructure containing ferrite, martensite, bainite, and retained austenite. The four alloys are SS1672, 38MnVS6, R350HT and SS2244. They are chosen to study the effect of increasing the Mn/Si ratio and the Cr effect on the microstructure. Multiphase steels with retained austenite of different fractions and morphologies in a ferritic-bainitic matrix have been obtained depending on the Cr and Si amounts. Detailed characterisation of the microstructural evolution of Q&P heat-treated four steel samples by optical microscopy (OM) was done only to provide a qualitative understanding. Despite these limitations, the OM micrographs were sufficient to confirm and identify the formed phases, especially the bainite phase. This study shows that high Si levels are not strictly required to suppress pearlite formation during the quenching and partitioning (Q&P) treatment of medium and eutectoid steels, due to the influence of manganese. A Mn/Si ratio greater than 2 is found to be essential for effectively preventing pearlite formation. Additionally, a lower martensite start temperature (M_s) significantly refines the microstructural features, particularly bainite and retained austenite.

Keywords: Quench and partitioning, Bainite, Martensite, Retained Austenite

Introduction

Multiphase steel is defined as steel that contains a mixture of different microstructural phases, typically including softer phases like ferrite and retained austenite, as well as harder phases such as martensite and hard microstructural constituents as bainite. This combination of phases is engineered to achieve a balance between strength and ductility[1-3]. Obtaining multiphase structures that combine both equilibrium and non-equilibrium phases typically involves carefully designed heat treatments and alloy compositions. Examples of these heat treatments are intercritical annealing followed by quenching to produce dual-phase steels (DP) with a microstructure consisting of ferrite and martensite phases[4,5]. Intercritical annealing followed by isothermal holding is a sophisticated heat treatment strategy used to produce TRIP steels with a microstructure that includes ferrite, martensite, and retained austenite phases[6]. Q&P is a sophisticated heat treatment technique used to produce high-strength steels with excellent ductility and formability by stabilizing retained austenite[7].

Multi-phase steels are designed to offer an optimal combination of strength and ductility by incorporating different phases within the steel microstructure that surpass those of conventional steels, which usually rely on a single strengthening mechanism like solid solution or precipitation hardening[8]. Conventional isothermal bainite transformation processes can indeed be very time-consuming, sometimes taking up to a month[9]. This lengthy process is primarily due to the slow kinetics of bainite transformation, which requires diffusion of carbon atoms within the steel

structure at relatively low temperatures. The initial presence of martensite promotes and speeds up the formation of bainite during isothermal treatment around the martensite start (M_s) temperature. This acceleration is often attributed to the creation of nucleation sites at the interfaces between martensite and austenite (α'/γ), a phenomenon sometimes referred to as the "swing-back" effect or mechanism[10-12]. The deviation of the alloy partitioning at the ferrite and martensite (α'/α) interface from the local equilibrium condition concentration is called para-equilibrium[13]. The C content in bainite formed at low transformation temperatures ($<450^\circ\text{C}$) is much higher than the para-equilibrium value, which is called the C supersaturation in bainite phenomenon. If there is a significant carbon supersaturation in bainite, it would generally hinder the transformation process because the excess carbon can impede the nucleation and growth of bainite. Thus, controlling carbon partitioning is crucial to avoid such supersaturation and to optimize the transformation kinetics. The assumption that carbon is in local equilibrium at the migrating interface means the absence of C supersaturation in the bainite. The presence of prior ferrite tends to accelerate martensite transformation because ferrite facilitates the nucleation of martensite. Conversely, prior ferrite can retard the bainite transformation due to its impact on local C concentrations[14].

In the literature, the roles of the alloying elements silicon and manganese in the development of multiphase microstructures in Q&P heat-treated steels are well documented individually. Si suppresses carbide formation during heat treatment, thereby enhancing the stability of retained austenite and promoting carbon partitioning [15,16]. Mn, on the other hand, serves as a strong austenite stabilizer by lowering the martensite start temperature (M_s), which increases the fraction of retained austenite at room temperature [17,18]. However, studies examining the combined effect of silicon and manganese are limited especially in medium and eutectoid steels.

This study aims to develop complex microstructures in four different steel alloys to obtain complex microstructure consisting of ferrite, bainite, martensite, and retained austenite through quenching and partitioning (Q&P) processing. A key aspect of the study is the role of the Si/Mn ratio in inhibiting carbide precipitation, thereby facilitating carbon partitioning into austenite instead of cementite formation. This study focuses on the effect of varying chemical compositions specifically involving conventional alloying elements such as C, Mn, Si, and Cr, which are commonly present in commercial steels like SS1672, 38MnVS6, R350HT, and SS2244, classified as medium-carbon and eutectoid steels on microstructural characterization after quenching and partitioning (Q&P) heat treatment using optical metallography

Materials and experimental procedure

Material

All the steel samples used in this study are categorized as low-alloy steel. Four alloys are used in this work the first three samples are medium C steel and the last sample is eutectoid steel and their compositions are shown in table 1. They are chosen to study the effect of increasing the Mn/Si ratio and the Cr effect on the microstructure. According to the empirical equations 1 and 2, the bainite starting temperature (B_s) and martensite starting temperature (M_s) can be calculated with alloying element concentrations expressed in weight percent[19,20]:

:

$$M_s = 498.99 - 333.3C - 33.3Mn - 27.8Cr - 16.7Ni - 11.1(Mo + Si + W)$$

1

$$B_s = 630 - 45Mn - 30Cr - 20Ni - 25Mo - 35Si - 15W - 40V$$

2

Cylindrical samples 51 mm in diameter and 51 mm in length are used in the heat treatment tests.

Table. 1. Chemical composition of steel (wt.%) used in this study.

	Sample 1	Sample 2	Sample 3	Sample 4
% wt	SS1672 hot rolled	38MnVS6 hot rolled	SS2244 (AISI 4140) hot rolled	R350HT hot rolled pearlitic steels
%C	0.46	0.38	0.4	0.75
%Mn	0.5	1.4	0.8	0.95
%Cr		0.3	0.95	0.15
%Si	0.25	0.4	0.23	0.35
%V		0.14		0.01
% Mo			0.2	
Mn/Si	2	3.5	3.5	2.7

Heat Treatment

Heat treatment, which leads to obtaining the multiphase structure requires quenching to different temperatures and subsequent isothermal bainite transformation. The use of high austenitization temperatures ensures that a complete and uniform austenite phase is formed before quenching. This can increase the amount of retained austenite, particularly in the areas between the martensitic laths, where carbon diffusion is slow[21]. Austenitization temperature of the steel used in the experiment is 1020 °C, for samples 1,2,3 and 900 °C, for sample 4 as R350HT is typically fully austenitic at approximately 900 °C. These temperatures are above the Ac3 temperature to ensure full austenitization before quenching[22]. The temperature was increased to the austenitization temperature at a heating rate of 5 °C/s and held for 30 min. After austenitization the samples were quenched to temperatures in the intercritical range of the samples and then were held at these temperatures for isothermal heat treatment at 900–800 °C for samples 1,2 and 3 and at 800-700 °C for sample 4. The samples were first quenched to temperatures below the eutectoid temperature at 600–500 °C. Subsequently, they were quenched to temperatures below the martensite start temperature (Ms) and held for isothermal treatments at 350–400 °C and 200–250 °C for Samples 1–3, and at 300–200 °C for Sample 4. This intermediate quench temperature, situated between the martensite start (Ms) and martensite finish (Mf) temperatures, promotes the formation of a controlled fraction of martensite, while retaining a significant amount of untransformed austenite[23]. The samples were heated to the partitioning temperature range of 600–500 °C and held for shorter partitioning times, all kept under 300 seconds. Finally the samples were quenched

to room temperature. The basic quenching and partitioning heat treatment process for the four samples is illustrated in Fig. 1.

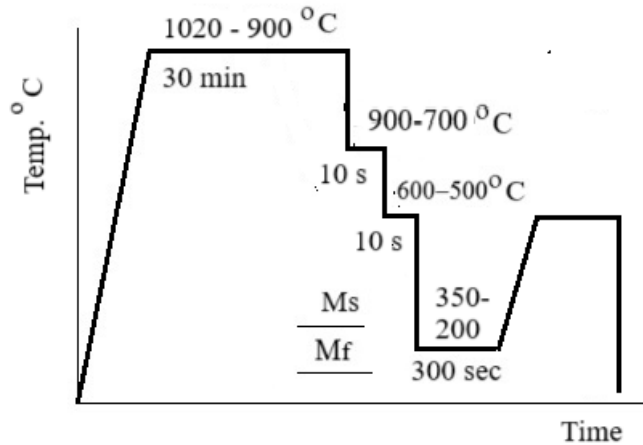


Figure 1. The basic route for the quenching and partitioning heat treatment process of the four samples

Microstructural Examination

Light metallography techniques have been widely used by researchers to differentiate retained austenite from other microconstituents in multiphase low-alloy steel microstructures[24,25]. These methods offer several advantages, such as ease of sample preparation and no restrictions on sample geometry, which is crucial for industrial applications where it is important to examine the entire sample to ensure uniformity of the microstructure. However, the most challenging when using light optical microscopy (LOM) is to distinguish finely divided retained austenite from martensite. For microstructural investigation in the light optical (LOM), the specimens were prepared by grinding with emery paper, polishing with diamond paste, and etching with 3% Nital (97ml ethanol, 3ml HNO₃). The microhardness was done in the ferrite and martensite phases individually. Optical metallography (OM) was used to perform microstructural characterization. Despite these limitations, the OM micrographs were sufficient to confirm and identify the formed phases, especially the bainite phase. The metallographical analysis were done using a Leica DMREM light optical microscope having high-performance LED illumination for analyzing in brightfield, darckfield, and phase contrast.

Results and Discussions

It is evident from Fig.1a that the microstructure of sample 1 is formed by three phases, allotriomorphic ferrite formed along the former austenite grain boundaries following their contours as indicated by the white regions. The dark grey regions (Fig. 1a) are pearlite. The light grey regions in Fig 1a are magnified and are presented in Fig.1b and the pearlite are magnified in Fig. 1c. The micro indent shown in Fig. 1a. measures the microhardness of multiple phases. The larger indents include pearlite and allotriomorphic phases and the smaller indents measures the hardness of multiple phases simultaneously namely martensite, bainite and allotriomorphic ferrite.

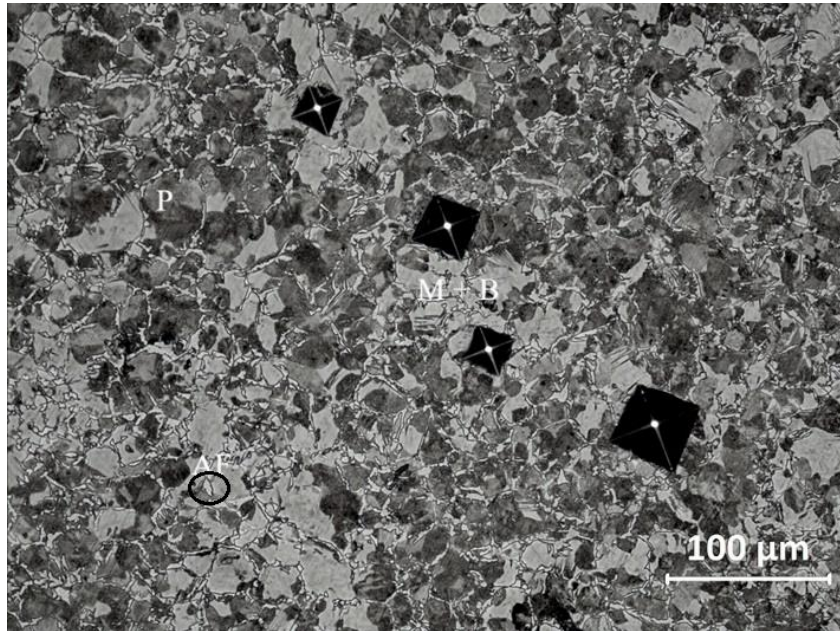


Figure.1a. Optical micrograph of sample1 showing showing pearlite, allotriomorphic and Widmanstätten ferrite.

Fig. 1b shows that the microstructure consists of allotriomorphic ferrite decorated at pre austenite grain boundaries(PAGB) and a mixture of bainite and martensite. It is observed in Figs. 1b and 1c that the interface between allotriomorphic ferrite and bainite is clear in some cases and unclear in the others. The interface is clear means that a black line is visible between two phases. At unclear interfaces between two phases suggests that there might be a gradual transition or mixing of orientations between the two phases. This could be due to partial transformation or overlap zones where the phase boundaries are not well-defined[26]. This can be caused by the fact that the interfacial energy and the grain boundary energy is not constant with the orientation of the interface and the grain boundary[27]. The interface between the allotriomorphic ferrite and pearlite is unclear, no boundary visible between allotriomorphic ferrite and pearlite. Optical microscope observation showed that the interfaces between allotriomorphic ferrite and adjacent bainite are mostly of the clear type which suggests they are high-angle boundaries.

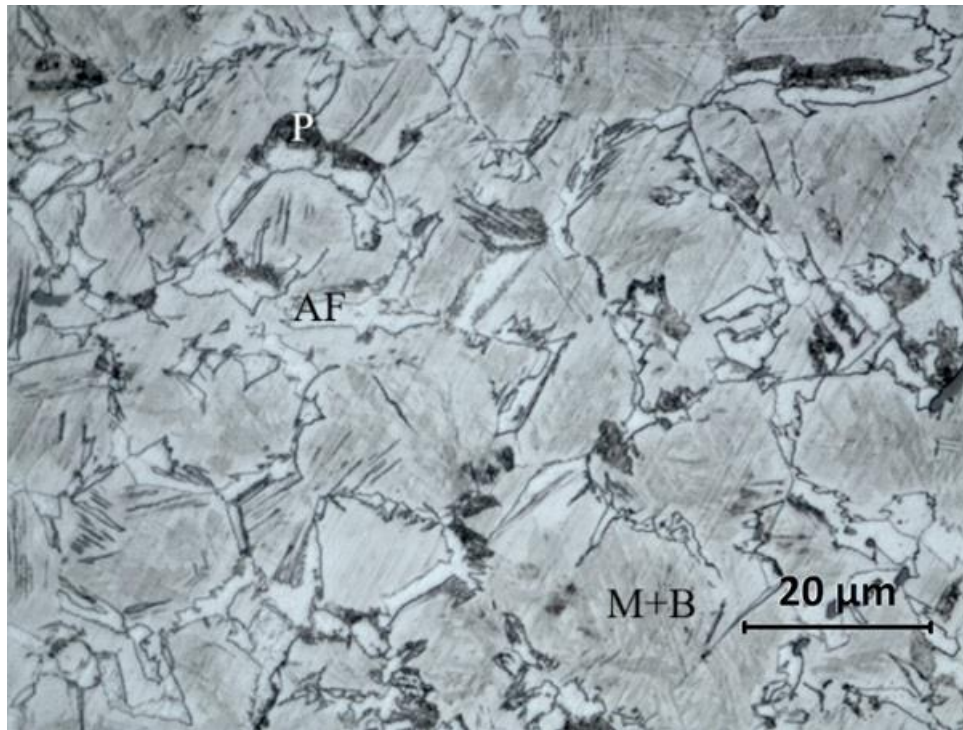


Fig.1b. Optical micrograph of sample 1 showing pearlite, bainite, martensite, and allotriomorphic ferrite.

When ferrite grows, the carbon that was previously in the austenite accumulates in the remaining austenite at the advancing planar ferrite fronts. If the carbon concentration becomes sufficiently high, cementite may form unless the reaction is prevented by kinetic factors.

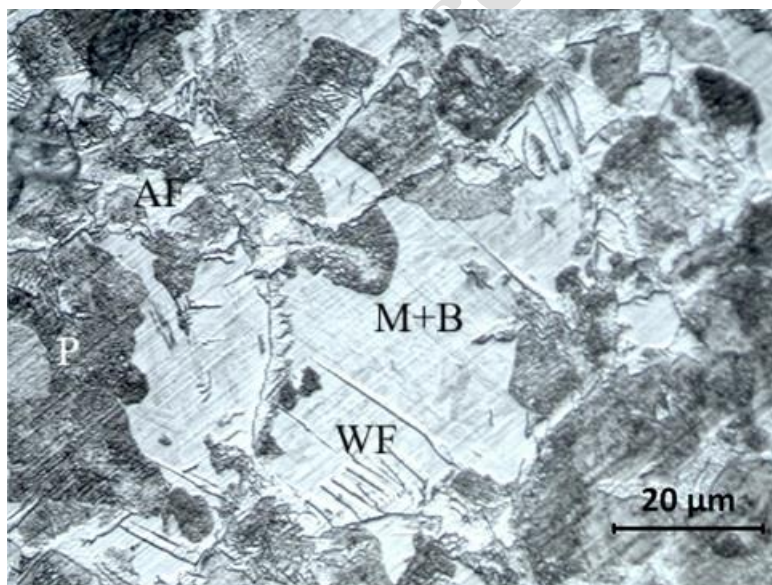


Fig.1c. Optical micrograph of sample 1 showing Widmanstätten ferrite, martensite, pearlite and allotriomorphic ferrite.

Some of the allotriomorphic ferrite (primary ferrite) at PAGBs have saw-teeth like morphology seen in Fig. 1c. Widmanstätten ferrite can sometimes form independently without the subsequent formation of pearlite, and dependently with the subsequent formation of pearlite under specific cooling conditions. This is because the cooling rate within the sample is not homogenous across the thickness of the sample[28]. All the Widmanstätten plates are parallel and have probably nucleated on the extension of the grain boundary shown in the lower right part of Fig. 1c. It can be seen from Fig. 1c that the upper ends of Widmanstätten are sharp denote the advancing edges of growth, while the lower ends are blunt indicating a rectangular cross-section of the plates.

The microstructure of sample 2 shown in Fig.2a is a typical OM image of the bainite formed at PAGB having feathery structures of parallel plates on both sides of the former austenite grain boundary which is a typical microstructure of upper bainite. Also there is intra granular nucleation of acicular bainite which are the short units of bainite nucleated on sides of primary units. Nital etching revealed the as-quenched martensite as a light-etching region containing acicular ferrite. Allotriomorphic ferrite formed at the PAGBs, hinders the nucleation of bainite at PAGBs. With the hindrance of bainite nucleation at the grain boundaries due to allotriomorphic ferrite, the steel's microstructure often shifts towards the formation of acicular ferrite within the austenite grains. In a mixed ferrite + austenite microstructure, both γ/γ grains and α/γ interface boundaries can act as nucleation sites for bainite[29]. According to the study done by Ravi et al.[30] the presence of the α/γ interface will result in a higher alloying gradient across the interface. The increased concentration of the alloying elements near the α/γ interface acts as a chemical retardation effect on the subsequent bainite transformation. The competition between acceleration (due to interface features) and retardation (due to higher alloying concentrations near the interface) determines the overall kinetics of bainite transformation in steels.

The initial banded microstructure of sample 2 can significantly impact the heat treatment process. Microstructural banding in hot-rolled low-carbon high-alloyed steels sample 2 arises due to the segregation of substitutional alloying elements during solidification. Sample 2 has a ferrite/pearlite banded microstructure in the as rolled condition and the banded structure is not evident after heat treatment. The absence of a banded microstructure after heat treatment does not mean that segregation is absent due to the fact that during austenitization the diffusion of substitutional alloying elements such as Cr or Mn is negligible. However, the structure of the α/γ interface, together with the associated chemical heterogeneity near the interface, including carbon and alloying element segregation, resulting from the nucleation of bainite[14] and the fact that in the context of microstructural banding, the phenomenon of austenite pancaking leads to increased total grain boundary area, which lead to a “geometrical dilution” of segregated elements. Also the homogenization of carbon across regions with varying manganese concentrations helps to ensure a more uniform microstructure, reducing the chances of banding. Since manganese (Mn) reduces the activity of C, it interacts with C in an attractive manner, leading to lower C activity when both elements are present in the matrix. As a result, C tends to accumulate in Mn-rich regions, resulting in higher local C concentrations. [31, 32]. The presence of bainite and Widmanstätten ferrite in Figs.2a and 2b suggests a non-uniform cooling rate or varying alloy composition within the steel. Comparing sample 1 with sample 2 exhibit a significant variation in their pearlite content (see Fig.1 and Fig. 2). The pearlite transformation is extremely sensitive to Mn this is seen in the

influence Mn has on the CCT diagram seen in Fig. 3. The CCT diagrams were created with the usage of JMatPro software because thick samples still undergo gradual cooling from the surface inward during the cooling stage following the isothermal hold. From Fig. 3 it can be seen that the pearlite curve is shifted towards longer times. Increasing Mn content tends to shift the phase transformation temperatures, making the formation of bainite more favorable compared to pearlite and ferrite. Higher Mn content stabilizes austenite at lower temperatures, which encourages the formation of bainite rather than Widmanstätten ferrite or pearlite as the steel cools. Cr reduces both the Ms and Bs temperatures as seen in eqs. 1 and 2, further it increases the amount of retained austenite[33]. The reduction of potential energy due to the attractive interactions between C-Cr and C-Mo in a C enriched prior austenite is driven by the formation of stable carbide phases. These interactions can decrease the carbon content that partition in retained austenite[34, 35]. This reduces the rate at which lower bainite forms because the diffusion of carbon, which is necessary for the formation of bainite, is hindered[36]. Si reduces the driving force for cementite and carbides nucleation and Si shifts the bainitic transformation towards a more ferritic structure with finer and more plate-like morphology[37-39]. This change in the microstructure is one of the reasons why bainite morphology becomes more refined and changes with increasing Si content. By stabilizing ferrite and reducing carbide formation, Si leads to an increased amount of carbon in the austenite phase, which in turn results in a higher amount of retained austenite.

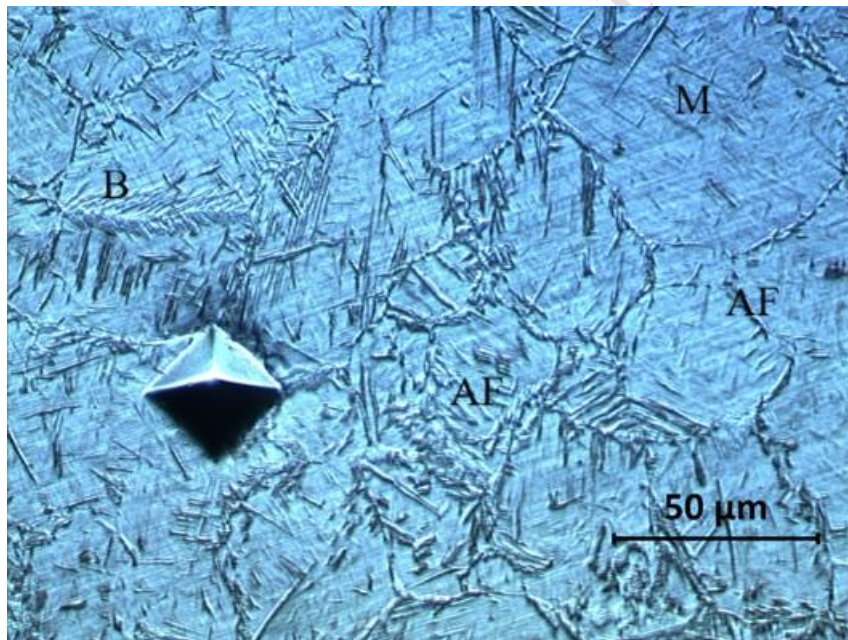


Figure 2a. Optical micrograph of sample 2 showing bainitic, martensite, acicular ferrite and allotriomorphic ferrite.

In Fig. 2b the intra granular shapes of the bainite-ferrite in the grains are sub-grains in the upper bainite. The bainitic ferrite plates can only grow to a certain length due to the constraints imposed by the transformation process and the presence of obstacles such as cementite particles or low-misorientation boundaries. Once these plates reach their maximum length, new plates or "subunits" of bainitic ferrite can nucleate that carries the growth further. These subunits are separated by low-misorientation boundaries or by cementite particles[40]. Nital etching revealed the as-quenched martensite as a light-etching region containing acicular ferrite.

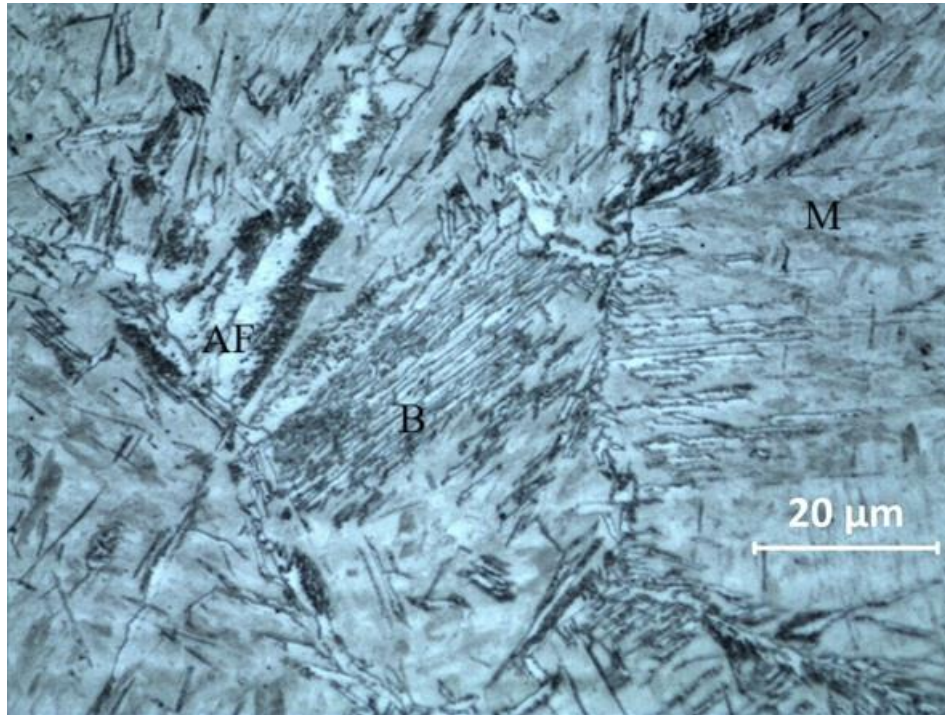


Figure 2b. Optical micrograph of sample 2 showing pearlite with allotriomorphic ferrite at prior austenite grain boundaries, bainite and martensite intra-granularly.

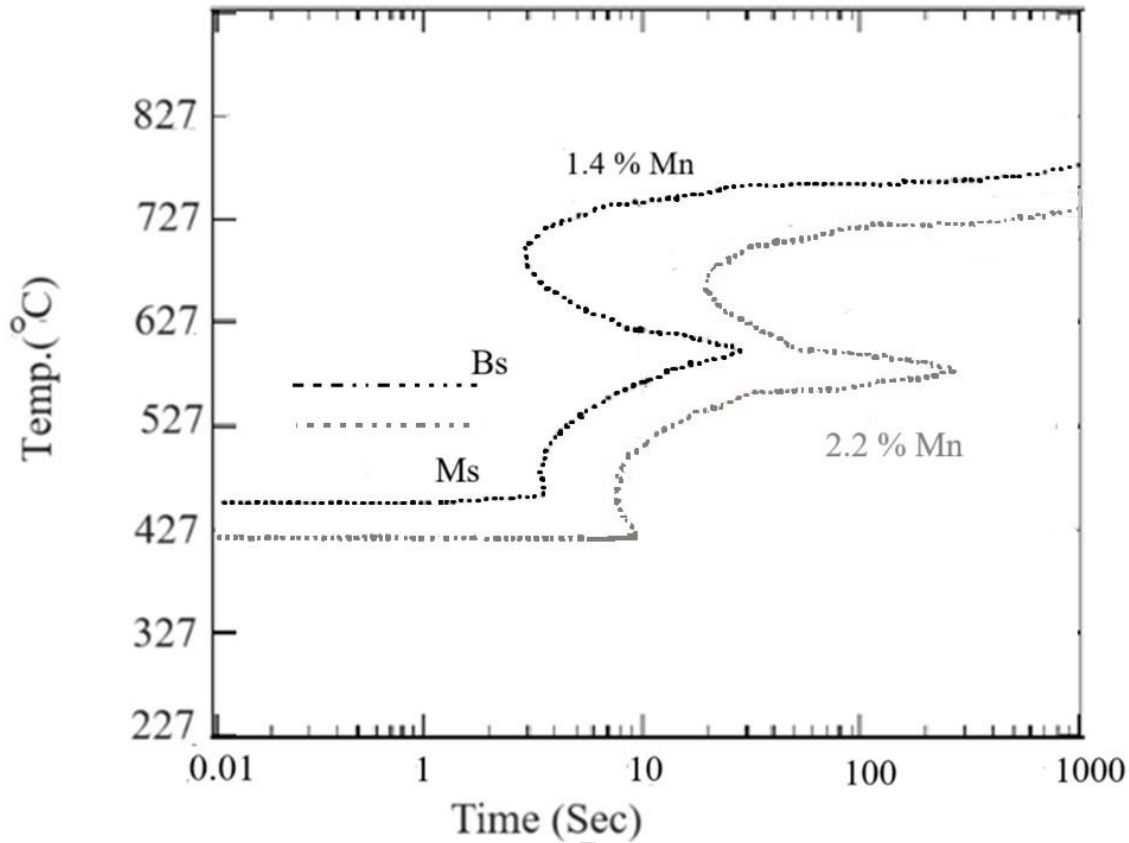


Figure 3. TTT diagram of sample 2 (38MnVS6 steel) created and calculated with the usage of JMatPro software.

Comparing the microstructure of sample 3 with all the other samples, the microstructure varies with the increase in Cr content of sample 3 compared to all the other samples. Figs 4a and 4b show no polygonal ferrite in sample 3 which leads to the conclusion that the amount of polygonal ferrite decreases with Cr addition. Cr segregates to the grain boundaries so the Cr atoms at the grain boundaries pin or fix these boundaries in place. This pinning effect impedes the movement of the grain boundaries as a result, the amount of polygonal ferrite formed decreases[41]. With the increase of Cr content as in sample 3, the polygonal (proeutectoid) ferrite gradually transforms to acicular ferrite, bainite and martensite.

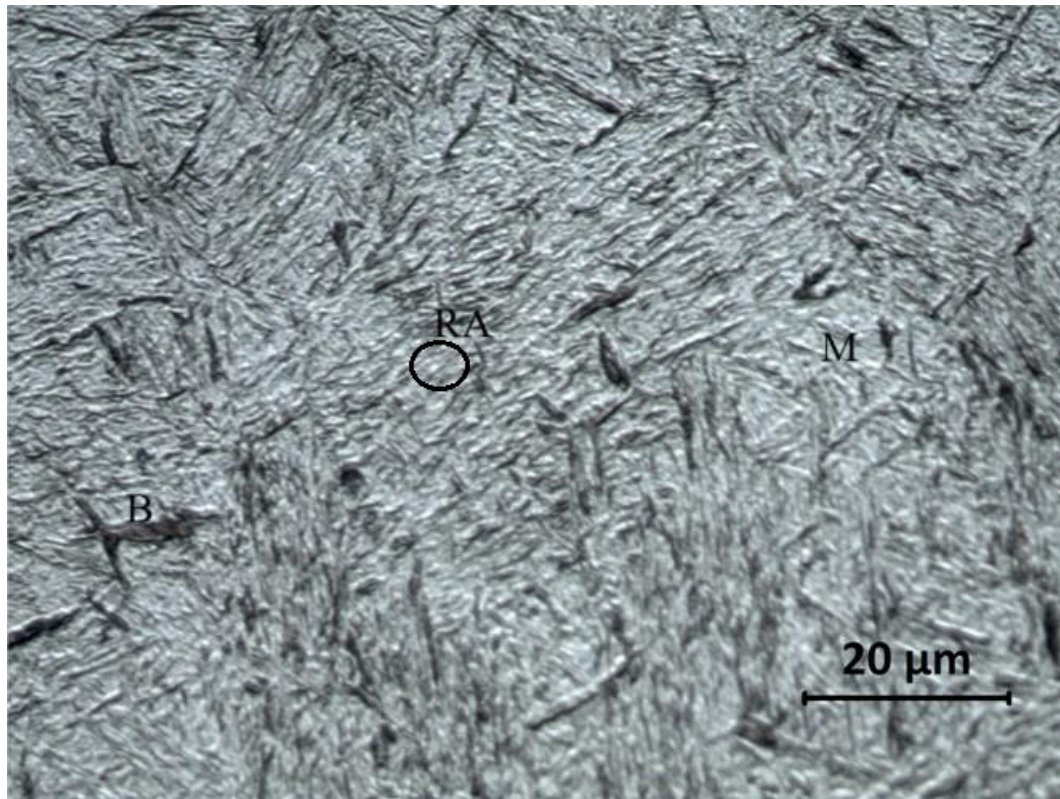


Fig. 4a. Optical micrograph of sample 3 at the surface showing bainite, martensite and small white islands RA with no polygonal ferrite present

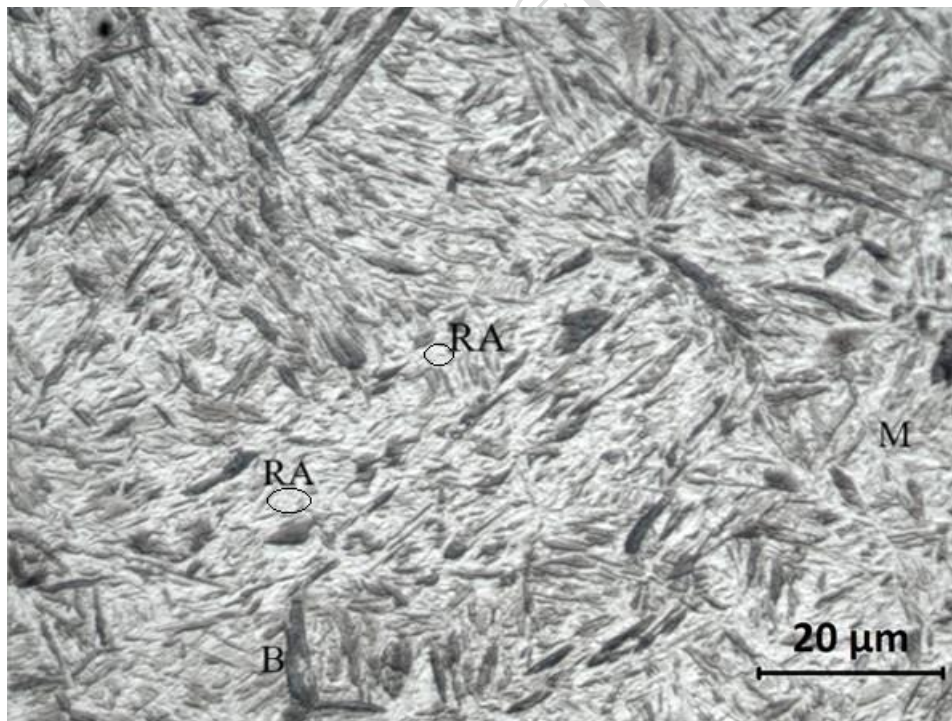


Fig. 4b. Optical micrograph of sample 3 at 5 mm from the surface showing bainite, martensite and very small white islands RA with no polygonal ferrite present

The OM observations revealed that sample 3 (Fig. 4a and 4b) and sample 4 (Fig. 5a and 5b) having the lowest M_s when quenched to just below M_s leads to lower isothermal bainite transformation temperatures which results in a significant refinement of the microstructure components bainite and RA. The microstructure of sample 3 and 4 is composed of bainite and RA in the form of thin layers and islands. As the isothermal temperature decreases, the bainitic ferrite plates become thinner and more closely spaced. This is because lower temperatures slow down the diffusion rates of carbon and other alloying elements, leading to the formation of finer, more compact bainitic ferrite plates. M/A islands tend to decrease in size and number as the transformation temperature lowers. This happens because the lower temperature leads to a finer and more homogeneous bainitic structure, reducing the areas where M/A islands can form.

Sample 4 was austenitized at 900 °C, this temperature is above the eutectoid temperature where the entire microstructure transforms into austenite. Fig. 5a. show typical lower bainite structure bainite at the former austenite grain boundaries also can be seen from Fig. 5a small white RA. At higher magnification the microstructure of the intragranular can be seen in Fig. 5b. RA (white) in the microstructure of sample 4 appear in the form of blocks and as thin films between ferrite plates seen in Figs. 5b. The blocks of RA are larger compared to the thin films. RA shown in Fig. 5b has an average size of few micrometers at the given magnification.

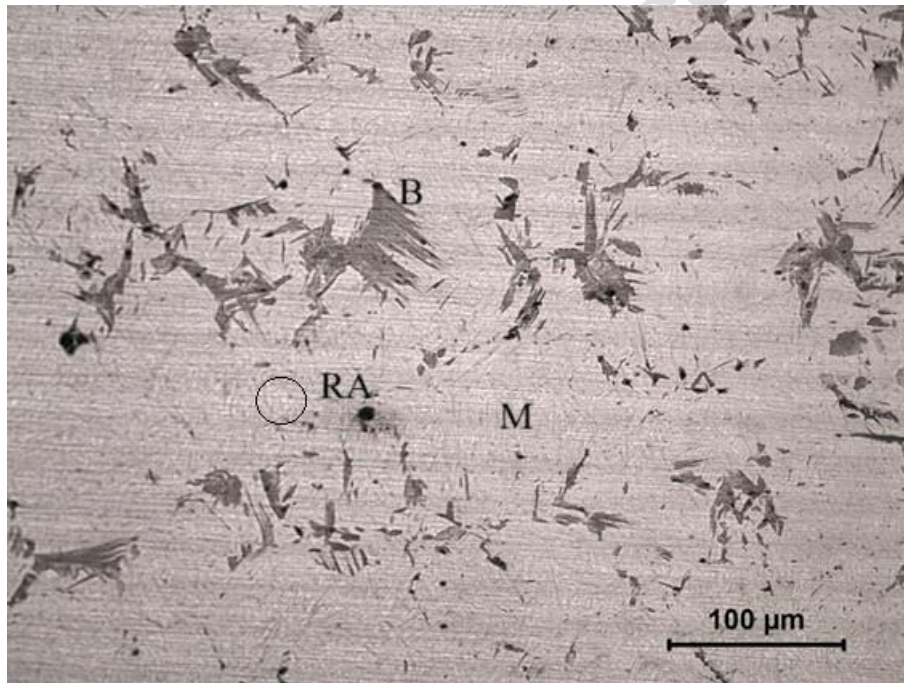


Figure 5a. Optical micrograph of sample 4 with visible areas where a bainitic structure was formed and small white RA.

RA in steel microstructures is a metastable phase and its morphology can vary significantly based on different process parameters. Lower isothermal quenching temperatures reduce the size of the bainite micro constituents. Because the transformation process is more rapid and less complete at lower temperatures, some austenite may remain as a film-like or retained phase within the bainite structure[42]. Higher isothermal temperatures result in slower transformation rates from austenite to bainite, wider bainite laths due to the enhanced diffusion of carbon, which facilitates the growth of these laths, and more stable RA, which tends to form larger regions rather than thin films. When temperature is too high, the enrichment of carbon in the residual austenite impairs the transformation of austenite into bainite. Subsequent quenching to room temperature after the isothermal bainite transformation can lead to the formation of martensite/austenite (M/A) islands in the microstructure. The analysis of the structures obtained from Fig.5b confirms that the RA often occurs between laths of bainitic ferrite as elongated, thin layers or fine grains.

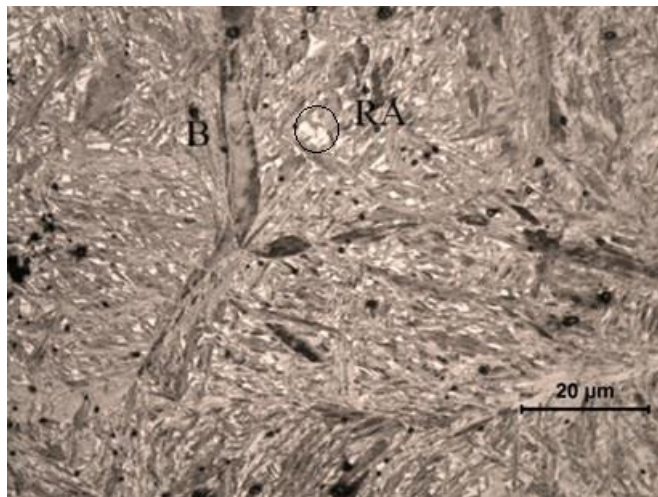


Figure 5b. Optical micrograph of sample 4 showing bainitic sheaves, RA as bright white and PAGB

A comparison of the microstructure and the M_s and B_s temperatures of sample 4 with sample 3, as shown in Table 1, reveals that the M_s and B_s temperatures are lower for sample 4. This is due to the higher carbon and alloying element content in sample 4 compared to sample 3. As a result, the bainitic transformation occurs at lower temperatures. Lowering the isothermal treatment temperature further promotes the bainitic transformation and reduces the amount of M/A islands. The microstructure of sample 4 consists of both film-like RA and island RA within the bainite structure, whereas the microstructure of sample 3 contains only island RA. According to the work done by Park et al. [43], the carbon content in retained austenite (RA) significantly impacts its stability. Film-like RA, which has a higher carbon content, is generally more stable than blocky RA with a lower carbon content. This increased stability in film-like RA is attributed to the higher carbon concentration in the austenite, which delays its transformation into other phases, such as martensite or carbide, during subsequent cooling or deformation.

When steel undergoes a Q&P treatment and the partitioning temperature is chosen to be between the M_s and room temperature, the resulting microstructure often includes a combination of phases such as martensite, bainite, and potentially retained austenite. These isothermal products are generally neither purely martensitic nor purely bainitic but rather a complex mixture of different phases. The distinction between product phases present is difficult particularly because they have similar morphologies. In Figs. 4a, 4b and 5b isothermal products with wide laths and wavy and irregular boundaries with ledges can be seen. According to Somani et al.[44] and Kim et al.[45], these isothermal products are neither purely martensitic nor purely bainitic. More recently, Somani et al. [44] identified this product phase as isothermal martensite. According to the literature, isothermal martensite is indeed predominantly reported in high-carbon steels and high-nickel alloys but not in hypoeutectoid and eutectoid steels[46-48].

The microstructure of multiphase steels containing martensite and ferrite is difficult to distinguish between bainite and martensite. Using the LOM methodology can contrast the different phases by fine-tuning the etching technique. Bainite typically has dark etching characteristics in metallographic images due to its specific phase structure. It can be seen from Figs.4 and 5 that martensite laths (dark units) appear during isothermal holding.

In summary, the four investigated steel alloys contain a certain amount of C, Si, Mn, Cr, Mo alloying elements. Sample 1 contains a specific Mn/Si ratio of 2 and undergoes a transformation of pearlite the other samples 2, 3, and 4, do not show any transformation of pearlite and they all have a Mn/Si ratio higher than 2. Isothermal heat treatment allows for significant microstructural refinement in bainitic steels. The Q&P process implemented in this study effectively stabilized retained austenite in samples 3 and 4, both of which exhibited the lowest M_s temperatures. A key factor in this outcome was the selected quench temperature, which facilitated the partial transformation of austenite into martensite. This process generated carbon-supersaturated martensite, acting as a carbon reservoir during the subsequent partitioning step. At the partitioning temperature, carbon diffused from the martensite into the remaining untransformed austenite. This carbon enrichment enhanced the thermal and mechanical stability of the austenite, increasing the likelihood of its retention at room temperature.

Conclusions

1. Samples 3 and 4 having the lowest M_s when quenched to just below M_s leads to lower isothermal bainite transformation temperatures, which results in a significant refinement of the microstructure components bainite and RA. Also, using steels with lower M_s is effective in minimization of competitive reactions, such as precipitation of carbides in austenite and formation of pearlite.
2. High Si levels are not strictly necessary to prevent pearlite formation during the Q&P treatment of medium and eutectoid steels, due to the presence of Mn. A Mn/Si ratio greater than 2 is found to be necessary to prevent pearlite formation.
3. Samples 2 and 3 have the same Mn/Si ratio of 3.5 but sample 3 has a higher Cr content of 0.95 % compared to 0.3 %. With the increase in Cr content for sample 3 the proeutectoid ferrite is Reduced and the microstructure mainly consists of lath bainite, martensite and RA.

Author Contributions statement:

Walid khraisat: writing, editing and microstructural analysis, methodology, deciding the heat treatment parameters

Data Availability

Data are available on request from the corresponding Author. The data that support the finding of this work are available upon request from the corresponding author walid khraisat.

Conflict of interest

The author of this work confirm that the manuscript have no conflict of interests to declare. And that the manuscript is the original work of the Author. Also there are no obstructions of publication, with respect to intellectual property.

References:

1. M. F. Carvalho, D. Centeno, G. Tressia, J. Avila, F. Cezario, A. Márquez-Rossy, E. Ariza, M. Masoumi, Development of a complex multicomponent microstructure on commercial carbon-silicon grade steel by governing the phase transformation mechanisms to design novel quenching and partitioning processing, *Journal of Materials Research and Technology*, 18 (2022) 4590- 4603. <https://doi.org/10.1016/j.jmrt.2022.04.066>.
2. H. Kawata, K. Hayashi, N. Sugiura, N. Yoshinaga, M. Takahashi, Effect of martensite in initial structure on bainite transformation, *Material Science Forum*, 638-642 (2010) 3307–3312 <https://doi.org/10.4028/www.scientific.net/msf.638-642.3307>
3. D. Edmonds, K. He, F. Rizzo, B. De Cooman, D. Matlock, J. Speer, Quenching and partitioning martensite—A novel steel heat treatment. *Material Science and Engineering.A.*, 438–440 (2006) 25-34. <https://doi.org/10.1016/j.msea.2006.02.133>
4. Q. Ren, S. Baik, D., An, D. Isheim, M. Zhu, B. Krakauer, D. Seidman, The effects of heat-treatment parameters on the mechanical properties and microstructures of a low-carbon dual-phase steel, *Material Science and Engineering A*, 888 (2023) 145801. <https://doi.org/10.1016/j.msea.2023.145801>
5. W. Khraisat, Strain hardening exponent and strain rate sensitivity exponent of dual-phase steels at quasi-static strain rates during tensile testing, *Cogent Engineering*, 10(2) (2023). <https://doi.org/10.1080/23311916.2023.2274548>
6. S. Li, R. Zhu, I. Karaman, R. Arróyave, Thermodynamic analysis of two-stage heat treatment in TRIP steels, *Acta Materialia*, 60(17) (2012) 6120-6130. <https://doi.org/10.1016/j.actamat.2012.07.054>.
7. L. Wang, J. Speer, Quenching and Partitioning Steel Heat Treatment, *Metallography, Microstructure, and Analysis*, 2 (2013) 268–281. <https://doi.org/10.1007/s13632-013-0082-8>
8. J. G. Speer, D. K. Matlock, B. C. De Cooman, J. G. Schroth, Carbon partitioning into austenite after martensite transformation. *Acta Materialia*, 51(9) (2003) 2611-2622. [https://doi.org/10.1016/S1359-6454\(03\)00059-4](https://doi.org/10.1016/S1359-6454(03)00059-4)
9. H. Guo, X. Feng, A. Zhao, Q. Li, J. Ma, Influence of prior martensite on bainite transformation, microstructures, and mechanical properties in ultra-fine bainitic steel, *Materials*, 12 (2019) 527. <https://doi.org/10.3390/ma12030527>

10. A. Navarro-López, J. Sietsma, M. J. Santofimia, Effect of prior athermal martensite on the isothermal transformation kinetics below m_s in a low-c high-si steel, *Metallurgical and Materials Transactions A*, 47 (2016) 1028-1039. <https://doi.org/10.1007/s11661-015-3285-6>
11. W. Gong, Y. Tomota, S. Harjo, Y. H. Su, K. Aizawa, Effect of prior martensite on bainite transformation in nanobainite steel. *Acta Materialia*, 85 (2015) 243-249. <https://doi.org/10.1016/j.actamat.2014.11.029>
12. L. Zhao, I. Qian, Q. Zhou, D. Li, T. Wang, Z. Jia, F. Zhang, J. Meng, The combining effects of ausforming and below- M_s or above- M_s austempering on the transformation kinetics, microstructure and mechanical properties of low-carbon bainitic steel, *Materials Design*, 183 (2019) 108123. <https://doi.org/10.1016/j.matdes.2019.108123>
13. G. Sheng, Z. G. Yang, Transition between partitioned and unpartitioned growth of proeutectoid ferrite in Fe-C-Xi systems. *Materials Science and Engineering A*, 465(1-2) (2007) 38-43. <https://doi.org/10.1016/j.msea.2007.04.051>
14. K. Zhu, H. Chen, J. P. Masse, O. Bouaziz, G. Gachet, The effect of prior ferrite formation on bainite and martensite transformation kinetics in advanced high-strength steels. *Acta Materialia*, 61(16) (2013) 6025. <https://doi.org/10.1016/j.actamat.2013.06.043>
15. M.J. Santofimia, L. Zhao, R. Petrov, J. Sietsma, Characterization of the microstructure obtained by the quenching and partitioning process in a low-carbon steel. *Material Characterization*, 59 (2008) 1758-1764. <https://doi.org/10.1016/j.matchar.2008.04.004>
16. S. Zhang, W. Zhou, Feng Hu, Serhii Yershov, Kaiming Wu, The role of Si in enhancing the stability of residual austenite and mechanical properties of a medium carbon bainitic steel, *Journal of Materials Research and Technology*, 30 (2024) 1939-1949. <https://doi.org/10.1016/j.jmrt.2024.03.189>
17. F. Shi, J. Zheng, J. Zhang, Y. Zhao, L. Chen, Heat Treatment Process, Microstructure, And Mechanical Properties of Spring Steel with Ultra-High Strength and Toughness. *Metals*, 14 (2024) 180.
18. Z. Nov, P. Salvetr, J. Kotous, P. Motyčka, A. Gokhman, Enhanced spring steel's strength using strain assisted tempering, *Materials* 15 (2022) 7354. <https://doi.org/10.3390/ma15207354>
19. E. Girault, The Developments of Cold-rolled TRIP-assisted Multiphase steels. Al-alloyed TRIP-assisted Multiphase Steels. Ph.D. Thesis. Katholieke Universiteit Leuven, 1999.
20. J. Zhao, C. Liu, Y. Liu, D. O. Northwood, A new empirical formula for the bainite upper temperature limit of steel. *Journal of Materials Science*, 36 (2001) 5045-5056. <https://doi.org/10.1023/A:1011874708194>
21. A. Stormvinter, Low Temperature Austenite Decomposition in Carbon Steels Ph.D. Thesis. Sweden: KTH Royal Institute of Technology, 1999.
22. V. Kurup, C. W. Siyasiya, R. J. Mostert, J. Wicks, The influence of full and partial austenitization temperatures on the quench and partition heat treatment process for advanced high strength steel, *OP Conf. Series: Materials Science and Engineering* 430 (2018) 012045. doi:10.1088/1757-899X/430/1/012045.
23. R. Jafari, S. Kheirandish, Sh. Mirdamadi, 2018. Effect of Q&P heat treatment on fine microstructure and mechanical properties of a low-alloy medium-carbon steel, 6th international biennial conference on ultrafine grained and nanostructured materials: (UFGNSM2017) AIP Conference Proceedings, 2018, 1920(1):020030. DOI: 10.1063/1.5018962.

24. G. F. Vander Voort, E. P. Manilova, Hints for imaging phases in steels, *Advanced materials & processes*, 163(2) (2005) 32-37.
25. L. Kučerová, K. Opatová, A. Jandová, Metallography of AHSS steels with retained austenite. *Microscopy and Imaging Science: Practical Approaches to Applied Research and Education*, Formatex Research Center: Badajoz, Spain, 2016, 455–463
26. H. Guo, Y. Bai, S. W. Yang, X. L. He, Nucleation of bainite on allotriomorphic ferrite/austenite interface in a low carbon steel. *Materials Science Forum*, 654–656 (2010) 2326-2329. <https://doi.org/10.4028/www.scientific.net/MSF.654-656.2326>
27. N. Rawashdeh, W. Khraisat, H. Borgström, Pinning effect of pores on grain growth in sintered steel, *Jordan Journal of Mechanical and Industrial Engineering*, 11(2) (2017) 73-78.
28. A. Borgenstam, M. Hillert, Phase transformations in steels fundamentals and diffusion-controlled transformations Volume 1 in Woodhead Publishing Series in Metals and Surface Engineering, 2012.
29. M. Oka, H. Okamoto, Variation of transition temperatures from upper to lower bainites in plain carbon steels, *Journal of Physics*, 5 (1995) 503-508. <https://doi.org/10.1051/jp4:1995877>
30. A. M. Ravi, A. Kumar, H. Herbig, J. Sietsma, M. J. Santofimia, Impact of austenite grain boundaries and ferrite nucleation on bainite formation in steels. *Acta Materialia*, 188 (2020) 424- 434. <https://doi.org/10.1016/j.actamat.2020.01.065>.
31. J. Mueller, D. Matlock, J. Speer, E. De Moor, Accelerated ferrite-to-austenite transformation during intercritical annealing of medium-manganese steels due to cold-rolling., *Metals*, 9(9) (2019) 926. <https://doi.org/10.3390/met9090926>
32. W. Khraisat, Tailoring of liquid phase sintering and microstructure of sintered steel', Ph.D. Thesis, Sweden: Chalmers University of Technology, Gothenburg, 2004, P 6-8
33. D. T. Pierce, D. R. Coughlin, K. D. Clarke, E. De Moor, J. Poplawsky, D. L. Williamson, B. Mazumder,, J. G. Speer, A. Hood, A. J. Clarke, Microstructural evolution during quenching and partitioning of 0.2C-1.5Mn-1.3Si steels with Cr or Ni additions, *Acta Materialia*, 151 (2019) 454-469. <https://doi.org/10.1016/j.actamat.2018.03.007>
34. M. Zhou, G. Xu, J. Tian, H. Hu, Q. Yuan, Bainitic Transformation and Properties of Low Carbon Carbide-Free Bainitic Steels with Cr Addition. *Metals*, 7(7), (2017) 263. <https://doi.org/10.3390/met7070263>
35. J. Tian, G. Xu, M. Zhou, H. Hu, X. Wan, The Effects of Cr and Al Addition on Transformation and Properties in Low-Carbon Bainitic Steels, *Metals*, 7(2) (2017) 40. <https://doi.org/10.3390/met7020040>.
36. L. Bracke, W. Xu, Effect of the Cr content and coiling temperature on the properties of hot rolled high strength lower bainitic steel. *ISIJ International*, 55(10) (2015) 2206-2211. <https://doi.org/10.2355/isijinternational.ISIJINT-2015-086>
37. S. Lin, A. Borgenstam, A. Stark, P. Hedström, Effect of Si on bainitic transformation kinetics in steels explained by carbon partitioning, carbide formation, dislocation densities, and thermodynamic conditions, *Materials Characterization*, 185 (2022) 111774. <https://doi.org/10.1016/j.matchar.2022.111774>.
38. W. Khraisat, H. Borgström, The Effect of the Si alloying method on the microstructure and properties of sintering and hardening of gray iron, *Metallography, Microstructure and Analysis*, 13 (2024) 595–600. <https://doi.org/10.1007/s13632-024-01108-8>

39. B. Kim, C. Celada, D. San Martín, T. Sourmail, R. del-Castillo, The effect of silicon on the nanoprecipitation of cementite, *Acta Materialia*, 61 (2013) 6983–6992. <https://doi.org/10.1016/j.actamat.2013.08.012>
40. J. Yin, M. Hillert, A. Borgenstam, Widening of laths in bainite. *Metallurgical and Materials Transactions*, 48 (2017) 5294–5303. <https://doi.org/10.1007/s11661-017-4316-2>
41. G. H. Zhang, M. Enomoto, Influence of crystallography on ferrite nucleation at austenite grain- boundary faces, edges, and corners in a Co-15Fe alloy, *Metallurgical and Materials Transactions A.*, 42(6) (2011) 1597–1608. <https://doi.org/10.1007/s11661-010-0554-2>
42. S. Chen, J. Hu, L. Shan, C. Wang, X. Zhao, W. Xu, Characteristics of bainitic transformation and its effects on the mechanical properties in quenching and partitioning steels, *Materials Science and Engineering A*, 803 (2021) 140706. <https://doi.org/10.1016/j.msea.2020.140706>.
43. H. S. Park, J. C. Han, N. S. Lim, J. B. Seol, G. G. Park, Nano-scale observation on the transformation behavior and mechanical stability of individual retained austenite in CMnSiAl TRIP steels, *Materials Science and Engineering A*, 627 (2015) 262-269. <https://doi.org/10.1016/j.msea.2015.01.005>
44. M. C. Somani, D. A. Porter, L. P. Karjalainen, R. D. Misra, Process design for tough ductile martensitic steels through direct quenching and partitioning, *Materials Today*, 2 (2015) 631-634. <https://doi.org/10.1016/j.matpr.2015.07.363>
45. D. Kim, S. J. Lee, B. De Cooman, Effect of Prior Athermal Martensite on the Isothermal Transformation Kinetics Below M_s in a Low-C High-Si Steel, *Metallurgical and Materials Transactions A*, 43 (2012) 1028-1039. <https://doi.org/10.1007/s11661-015-3285-6>
46. Y. Adachi, K. Hakata, K. Tsuzaki, Crystallographic analysis of grain boundary Bcc-precipitates in a Ni–Cr alloy by FESEM/EBSD and TEM/Kikuchi line methods, *Materials Science and Engineering A*, 412(1-2) (2005) 252-263. <https://doi.org/10.1016/j.msea.2005.09.033>
47. H. Landheer, S. E. Offerman, R. H. Petrov, L. A. Kestens, The role of crystal misorientations during solid-state nucleation of ferrite in austenite, *Acta Materialia*, 57(5) (2009) 1486-1496. <https://doi.org/10.1016/j.actamat.2008.11.034>
48. A. Béché, H. S. Zurob, C. R. Hutchinson, Analysis for kinetics of ferrite growth due to isothermal decarburization of austenite in the binary Fe–C system, *Metallurgical and Materials Transactions A*, 38(11) (2007) 1896-4. <https://doi.org/10.2320/matertrans.M2012161>

Figure.1a. Optical micrograph of sample1 showing showing pearlite, allotriomorphic and Widmanstätten ferrite.

Fig.1b. Optical micrograph of sample 1 showing pearlite, bainite, martensite, and allotriomorphic ferrite.

Fig.1c. Optical micrograph of sample 1 showing Widmanstätten ferrite, martensite, pearlite and allotriomorphic ferrite.

Figure 2a. Optical micrograph of sample 2 showing bainitic, martensite, acicular ferrite and allotriomorphic ferrite.

Figure 2b. Optical micrograph of sample 2 showing pearlite with allotriomorphic ferrite at prior austenite grain boundaries, bainite and martensite intra-granularly.

Figure 3. TTT diagram of sample 2 (38MnVS6 steel) created and calculated with the usage of JMatPro software.

Fig. 4a. Optical micrograph of sample 3 at the surface showing bainite, martensite and small white islands RA with no polygonal ferrite present

Fig. 4b. Optical micrograph of sample 3 at 5 mm from the surface showing bainite, martensite and very small white islands RA with no polygonal ferrite present

Figure 5a. Optical micrograph of sample 4 with visible areas where a bainitic structure was formed and small white RA.

Figure 5b. Optical micrograph of sample 4 showing bainitic sheaves, RA as bright white and PAGB